Magnetotransport in type-enriched single-wall carbon nanotube networks

X. Wang, W. Gao, X. Li, Q. Zhang, S. Nanot, E. H. Hároz, J. Kono, and W. D. Rice

Phys. Rev. Materials **2**, 116001 — Published 6 November 2018

DOI: 10.1103/PhysRevMaterials.2.116001

Magneto-Transport in Type-Enriched Single-Wall Carbon Nanotube Networks

X. Wang,[1,2] W. Gao,[1] X. Li,[1] Q. Zhang,[1] S. Nanot,[3,1] E. H. Hároz,[4,1] J. Kono,[1,5,6] and W. D. Rice[7,1,5,*]

[1]*Department of Electrical and Computer Engineering, Rice University, Houston, Texas 77005, USA*
[2]*Beijing National Laboratory for Condensed Matter Physics, Institute of Physics, Chinese Academy of Sciences, Beijing, 100190, China*
[3]*Laboratoire Charles Coulomb, Université de Montpellier, Campus Triolet, Place Eugne Bataillon - CC074, F-34095 Montpellier Cedex 5, France*
[4]*Explosive Sciences and Shock Physics Division, Los Alamos National Laboratory, Los Alamos, New Mexico 87545, USA*
[5]*Department of Physics and Astronomy, Rice University, Houston, Texas 77005, USA*
[6]*Department of Materials Science and NanoEngineering, Rice University, Houston, Texas 77005, USA*
[7]*Department of Physics and Astronomy, University of Wyoming, Laramie, WY 82071, USA*

(Dated: October 11, 2018)

Single-wall carbon nanotubes (SWCNTs) exhibit a wide range of physical phenomena depending on their chirality. Nanotube networks typically contain a broad mixture of chiralities, which prevents an in-depth understanding of SWCNT ensemble properties. In particular, electronic-type mixing (the simultaneous presence of semiconductor and metallic nanotubes) in SWCNT networks remains the single largest hurdle to developing a comprehensive view of ensemble nanotube electrical transport, a critical step towards their use in optoelectronics. Here, we systematically study temperature-dependent magnetoconductivity (MC) in networks of highly enriched semiconductor and metal SWCNT films. In the semiconductor-enriched network, we observe two-dimensional variable-range hopping conduction from 5 to 290 K. Low-temperature MC measurements reveal a large, negative MC from which we determine the wavefunction localization length and Fermi energy density of states. In contrast, the metal-enriched film exhibits positive MC that increases with decreasing temperature, a behavior attributed to two-dimensional weak localization. Using this model, we determine the details of the carrier phase coherence and fit the temperature-dependent conductivity. These extensive measurements on type-enriched SWCNT networks provide new insights that pave the way for the use of SWCNTs in solid-state devices.

Single-wall carbon nanotubes (SWCNTs) are rolled-graphene, one-dimensional, cylindrical crystals that show remarkable electronic, optical, magnetic, and thermal behaviors, such as ultra-high current carrying capacities[1], exciton-dominated absorption[2–4], long quantum coherence lengths[5,6], large Young's moduli[7], proximity-induced superconductivity[8], and giant thermal conductivities[9,10]. These physical properties stem from the rolling orientation of the underlying graphene sheet that forms the nanotube[11]: for certain wrapping angles (chiralities), the nanotubes are semiconducting, while for other orientations, the nanotubes are metallic or narrow-bandgap semiconductors. Beyond impressive physical behaviors, SWCNTs have an all-carbon composition and, thus, a very low mass density ($\sim$1.3 g/cm^3, as compared to $\sim$9 g/cm^3 for copper). However, the promise of various nanotube-based technologies continues to be hampered by the inability to transition from well-understood, single-nanotube experiments to macroscopic SWCNT networks. At the ensemble scale, nanotube network properties are complicated by defects, accidental dopants, inter-nanotube junctions, physical deformations, mixtures of different electronic types, random orientation, and non-nanotube materials.

Electrical and thermal transport behavior in SWCNT networks differs considerably from conduction in individual nanotubes. For instance, charge carriers in individual nanotubes exhibit quantum effects, such as quantum conductance and conductance fluctuations[6,12], which are not observed in nanotube ensembles. Indeed, since (macroscopic) translational invariance is absent in SWCNT networks, carriers encounter electrical potentials created via nanotube terminations, different nanotube species, and a lack of crystal orientation (i.e., no alignment). Consequently, it is unsurprising that electrical transport in seemingly similar SWCNT ensembles show a broad array of behaviors, including fluctuation-induced tunneling[13,14], weak localization[13,15–17], strong localization[16], metallicity[18], and Coulomb gap opening[17,19]. Beyond the absence of translation invariance, SWCNT ensembles also suffer from electronic type mixing: that is, SWCNT ensembles contain *both* semiconductor and metal nanotubes, which significantly confounds electrical and thermal measurement results. Recently, a new generation of type-enriched nanotube films[17] and heavily doped fibers[20,21] have been used in electrical transport measurements to provide more insight into the conduction mechanism of SWCNT ensembles. Unfortunately, none of these works present a complete study of temperature- and field-dependent conductivity, which prevents a comprehensive understanding of transport in SWCNT ensembles.

In this work, we investigate temperature- (T-) dependent magneto-transport of pristine SWCNT ensembles and semiconductor- and metal-enriched SWCNT films to reveal the underlying electrical transport mechanism in SWCNT networks. Measurements of pristine and semiconductor-enriched SWCNT conductivity, σ, show that electrical conduction follows a two-dimensional (2D) variable-range hopping (VRH) conduction over a broad

temperature range. When a magnetic field, B, is applied, we observe a large, negative, T-dependent magnetoconductivity (MC) signal, from which we determine both the localization length of the hopping-like species and the density of states at the Fermi energy. Unlike the strongly localized carrier transport in the semiconductor-dominated nanotube networks, the metal-enriched film exhibits two-dimensional weak localization (2DWL) behavior. We use this model to describe the electrical transport behavior of metal-enriched SWCNT ensembles. Our extensive measurements and thorough data modeling provide new insights into the carrier transport mechanisms in nanotube ensembles.

For the electrical transport experiments presented here, we prepared a set of three SWCNT networks with different semiconductor-to-metal nanotube ratios. We used nanotubes that either had no electronic-type enrichment ('pristine') or contained high concentrations of semiconductor ('semiconductor-enriched' or s-SWCNTs) or metallic ('metal-enriched' or m-SWCNTs) nanotubes. The pristine sample was prepared using acid-purified, laser-oven SWCNTs that were first sonicated and then centrifuged to form a pellet from which a small piece was cut and then mounted to a glass slide (see[22,23] for details about the nanotube composition). The electrical conductivity was measured in a four-point probe configuration (current source, voltage probe) to mitigate contact resistance effects. We silver painted the ends of the pelleted sample to source current through the entire sample, while gold contacts (spaced ∼1 mm apart) were sputtered on the three sides of the parallelepiped sample for voltage measurements.

To prepare the semiconductor- and metal-enriched nanotube films, we performed density gradient ultracentrifugation[25,26] on arc-discharge SWCNTs, following Yanagi et al.[27] and Hároz et al.[4,28]. Next, both the semiconductor- and metal-enriched suspensions were vacuum-filtered, dried, washed, and then transferred to a sapphire substrate after which gold contacts (spaced ∼3 mm apart) were sputtered onto the thin films; see Zhang et al.[24] for details regarding the film preparation. The s-SWCNT film was 410 nm thick, while the m-SWCNT film was 190 nm thick. X-ray photoelectron spectroscopy of the prepared nanotube films revealed that adsorbed gaseous species, such as nitrogen and oxygen, were present. To remove these molecules, all three nanotube samples were vacuum annealed for several hours.

We evaluated the composition and purity of the semiconductor- and metal-enriched SWCNT networks using several characterization techniques, such as optical absorption, photoluminescence excitation spectroscopy, profilometry, and resonant Raman spectroscopy. Figure 1a shows a scanning electron microscope image of the deposited, enriched nanotube bundles in a film. Images like this one indicate that after processing, the average nanotube length is several hundred nanometers, which is in line with other estimates of enriched SWCNTs[29,30].

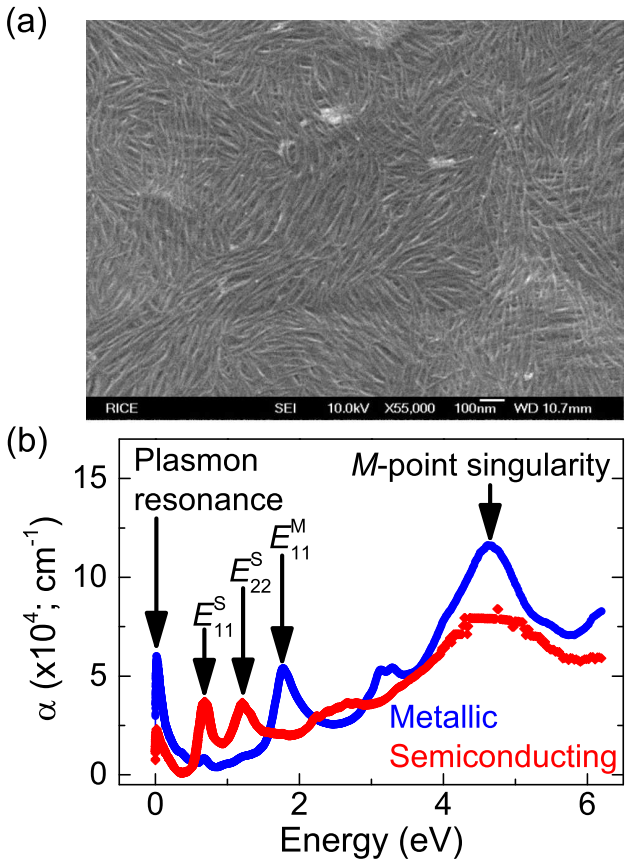

FIG. 1. (a) Scanning electron microscope image of SWCNT networks. The films used for electrical transport experiments were washed to remove surfactants and thermally annealed to remove adsorbed species. (b) Absorption of the post-annealed metal-enriched (blue) and semiconductor-enriched (red) SWCNT films[24]. The difference in absorption clearly show the presence of distinct SWCNT electronic types, which in combination with other characterization techniques, allow us to conclude that the films were highly type enriched.

Despite the well-resolved excitonic transitions seen in the films, electron microscopy shows that the SWCNT bundles are in close, intimate contact with one another.

Figure 1b shows the optical absorption of both the semiconductor- and metal-enriched SWCNT films from 0.9 meV to 6 eV[24]. In both cases, the low energy absorption spectrum is dominated by the plasmon resonance[24], while the high-energy region (>4 eV) shows the so-called M-point singularity created by the saddle-point exciton[31]. For this work, the most important absorption data falls in the region from 0.5 to 3 eV, where nanotube electronic transitions occur[32]. In this regime, the absorption from pristine SWCNTs contains numerous strong excitonic absorption transitions[3,33]; in contrast, the type-enriched samples have only specific exciton peaks, which reflects the suppression of the metallic (semiconductor) species in the semiconductor- (metal-)enriched fractions.

Four-point probe T- and B-dependent conductivity experiments on the three SWCNT networks were performed

in a helium-flow magnet (either a Janis 6 T or an Oxford 10 T system) using dual lock-in amplifiers. To avoid sample heating, we kept the source current at or below 100 μA. As seen in the inset of Fig. 2a, $I-V$ curves were taken at several temperatures from 1.5 to 300 K to ensure that we were in the linear regime: at low temperatures, we observe the $I-V$ curve becomes non-linear above a source current of 2 mA. For all measurements, the field was applied perpendicular to both the plane of the sample and the direction of the current.

We first consider the electrical transport in the pristine SWCNT ensemble. Figure 2a shows $\sigma\,(T)$ for the pristine SWCNT network across a broad temperature range. As with other work on pristine SWCNT ensembles[13,15,16,34], σ decreases with T from 350 K to 1.5 K, exhibiting a four-fold reduction in this temperature range. Despite the fact that $\frac{d\sigma}{dT}>0$ for all T, the nature (weak or strong) and source of the localization is complex, having contributions from a lack of long-range order, the presence of metallic and semiconducting nanotubes, SWCNT impurities, dislocations, and defects, and the physics of bundling (i.e., intimately contacted nanotubes).

The T-dependent MC $\left[=\frac{\sigma(B,T)-\sigma(0,T)}{\sigma(0,T)}\right]$ measurements shown in Figures 2b and 2c suggest at least two separate temperature regimes: above ≈7 K the MC is increasingly *positive* as T decreases, while below ≈7 K, the MC becomes increasingly *negative* with lower T and higher B. Previous MC measurements in unsorted nanotubes[15,16,35] and intentionally doped semiconductors[36–38] have shown very similar T-dependent MC behaviors. Given the complex behavior of the T-dependent MC, a large variety of transport models that have both positive and negative MC components can be used to explain this data.

Instead of attempting to computationally de-convolute the different transport processes occurring in the pristine sample, we eliminated the largest confounding factor (electronic-type mixing) by performing T-dependent MC measurements on type-sorted SWCNT networks. Figure 3a shows the T-dependent conductivities of SWCNT films with different ratios of metallic to semiconducting nanotubes. As expected, we observe that as the SWCNT metal-to-semiconductor ratio decreases, so does the conductivity. The conductivity of the s-SWCNTs drops by two orders of magnitude from 300 to 5 K, which is a much larger decrease than in the pristine film. This large conductivity decrease suggests that the s-SWCNT network contains markedly fewer conducting pathways than the pristine ensemble.

Despite its metallic nature, the m-SWCNT film also exhibits a decrease in conductivity with temperature, which indicates some degree of localization. However, in contrast to the pristine and s-SWCNT films, the m-SWCNT film changes by less than a factor of two when T is varied between 300 and 5 K. Unlike other studies on T-dependent conductivity in SWCNT ensembles[13,16,18,20], we do not observe a change in the sign of $\frac{d\sigma}{dT}$ as we move from high to low temperatures. This lack of negative

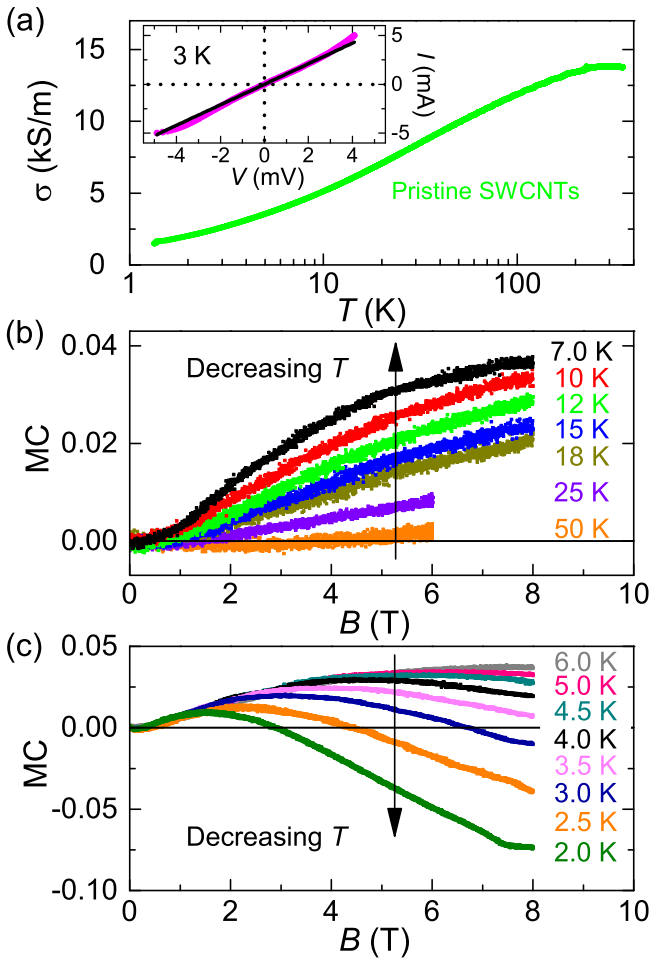

FIG. 2. (a) T-dependent conductivity for the pristine SWCNT ensemble. The conductivity monotonically decreases with decreasing T. Inset: $I-V$ curve (magenta dots) for the pristine SWCNT sample at 3 K. Only at sourced currents below ∼1.5 mA does the $I-V$ curve behave linearly (black line fit). T-dependent MC for (b) 7.0 to 50 K and (c) 2.0 to 6.0 K. At high T, the MC is positive, transitioning from linear with B to sub-linear as T is lowered. When T drops below 7.0 K, we begin to see that the sub-linear behavior observed at higher temperatures is caused by a negative MC contribution, which dominates the MC at high B and low T.

$\frac{d\sigma}{dT}$ in the m-SWCNT film may suggest a high degree of nanotube disorder in our films, which could be caused by the shorter-than-normal nanotubes created by our type-enrichment procedure.

We now turn our attention to the electrical transport in s-SWCNT networks. It should be noted from the outset that defects present in semiconductor SWCNTs, as well as remnant metallic and narrow-bandgap SWCNTs, can create localized conductive sites that facilitate electrical transport in a nominally insulating film. This situation is similar to electrical measurements made on polymers[39,40], doped semiconductors[38,41], and granular media[42], whereby carriers move between localized states of differing energies spaced at varying distances apart

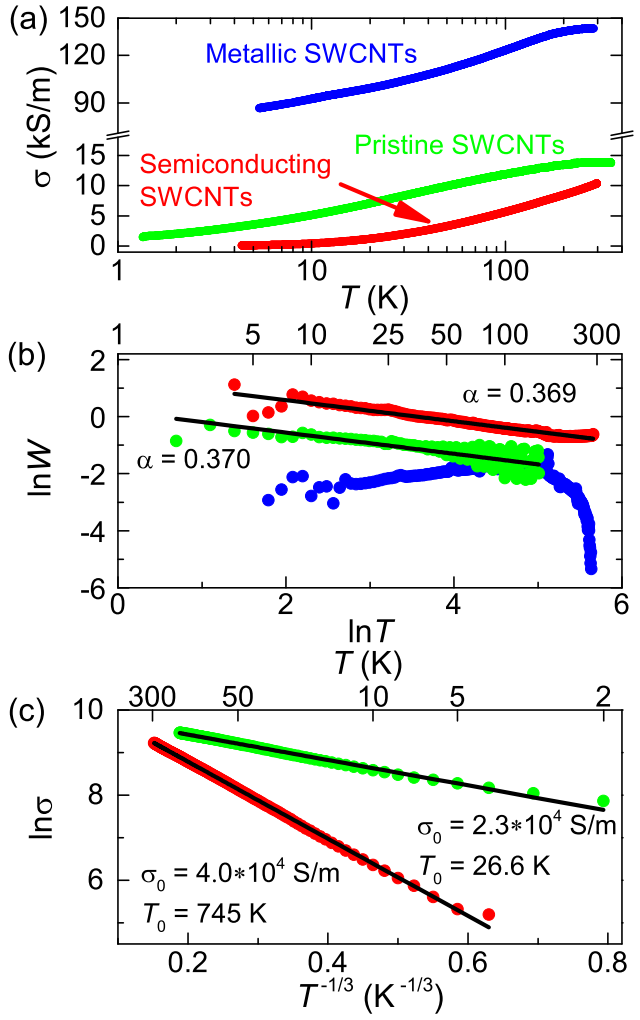

FIG. 3. (a) T-dependent conductivity for the pristine (green), metal- (blue), and semiconductor-enriched (red) SWCNT ensembles. Consistent with expectations, as the metallicity of the samples increases, so does the conductivity. (b) $\ln W$ as a function of $\ln T$ for each of the three samples. The slope, $\frac{\partial \ln W}{\partial \ln T}$, is equal to $-\alpha$, which we find to be -0.370 ($d = 1.70 \simeq 2$) for pristine SWCNTs and -0.369 ($d = 1.71 \simeq 2$) for s-SWCNTs. As seen by positive slope of $\ln W$, the m-SWCNT conductivity clearly does not follow a VRH behavior. (c) $\ln \sigma$ as a function $T^{-1/3}$ for the pristine and s-SWCNT samples. Two-dimensional VRH describes the pristine and s-SWCNT network conductivity across a broad temperature range.

(i.e., transport between non-adjacent sites). This transport behavior, known as VRH, is a competition between energy-state differences and spatial separation that produces a T-dependent conductivity first investigated by Mott[43,44]:

$$\sigma(0,T) = \sigma_0 \exp\left[-\frac{T_0}{T}\right]^{\alpha}. \quad (1)$$

Here α depends on the particular hopping mechanism, while σ_0 (high-temperature conductivity limit) and T_0 are T-independent variables. T_0 can provide deep insights into the system under study, since $T_0 = \frac{13.8}{k_B \xi^2 N(E_F)}$ in 2D[45], where ξ is the wavefunction localization length, $N(E_F)$ is the density of states at the Fermi energy, E_F, and k_B is the Boltzmann constant. In Mott-like VRH, $\alpha = 1/(1+d)$, where d is the dimensionality of the system. Given the complexity of Eq. 1 and the difficulty of accurately determining α (and thus, d), we calculate W, which is defined as[16]: $W = \frac{\partial \ln \sigma}{\partial \ln T} = \alpha \left(\frac{T_0}{T}\right)^{\alpha}$. The slope of $\ln W$ as a function of $\ln T$, which is graphically depicted in Fig. 3b, is equal to $-\alpha$ providing us with a route for unambiguously determining the system dimensionality. For the pristine SWCNT ensemble, we find $\alpha = 0.370$ from 2 to 110 K, which translates into a dimensionality, d, of 1.70, while for the s-SWCNT film, $\alpha = 0.369$ ($d = 1.71$) from 4 to 286 K (full temperature range). Given these values for d, we consider conduction for both samples to be 2D VRH. In contrast to the primarily semiconductor SWCNT ensembles, the behavior of $\ln W$ for the m-SWCNT film has the opposite sign for α, confirming that the m-SWCNT conductivity cannot be described as VRH conduction; we note that a similar finding using W-parameter analysis was seen by Vavro et al. in doped SWCNT ensembles[16].

Using $d = 2$, we have plotted and fit the natural log of the conductivity as a function of $T^{-1/3}$ for both the pristine and s-SWCNT samples in Fig. 3c. As can be seen by the fitting, we find that the data can be very well described by 2D VRH conduction in the low temperature regime with $T_0 = 26.6$ K and 745 K for pristine and s-SWCNTs, respectively. The excellent agreement of $\sigma(0,T)$ with 2D VRH agrees with previous observations by Vavro et al.[16] and Kim et al.[15], but diverges with data presented by Jaiswal et al.[19] and Yanagi et al.[17] who suggest that a soft Coulomb gap opens around the Fermi energy at lower temperatures. Prompted by these previous results, we closely examined $\sigma(0,T)$ at low temperatures (<20 K), but never observed Efros-Shklovskii VRH[46] (α=$\frac{1}{2}$) for either the pristine or s-SWCNT networks.

A deeper understanding of this strongly localized conduction behavior can be gained from T-dependent MC. For this work, we focus on the low-T (2 to 10 K) behavior of the s-SWCNT films where the most significant MC changes are observed (see Fig. 4a). At very low fields (B<0.5 T), the MC is positive and small. Above 0.5 T, the MC becomes negative for temperatures below 10 K. The negative MC behavior increases with decreasing T, reaching $\sim$−0.35 at 2 K, 10 T; this MC magnitude is over four times greater than the MC change seen in the pristine SWCNT network. Additionally, unlike MC in the pristine SWCNTs, the MC for the semiconductor-enriched network continually decreases with lower temperature, similar to previous work on annealed nanotube buckypapers[16] and partially semiconductor-enriched nanotube networks[19].

To more fully understand our MC data, we focus on two key processes within the strong localization paradigm

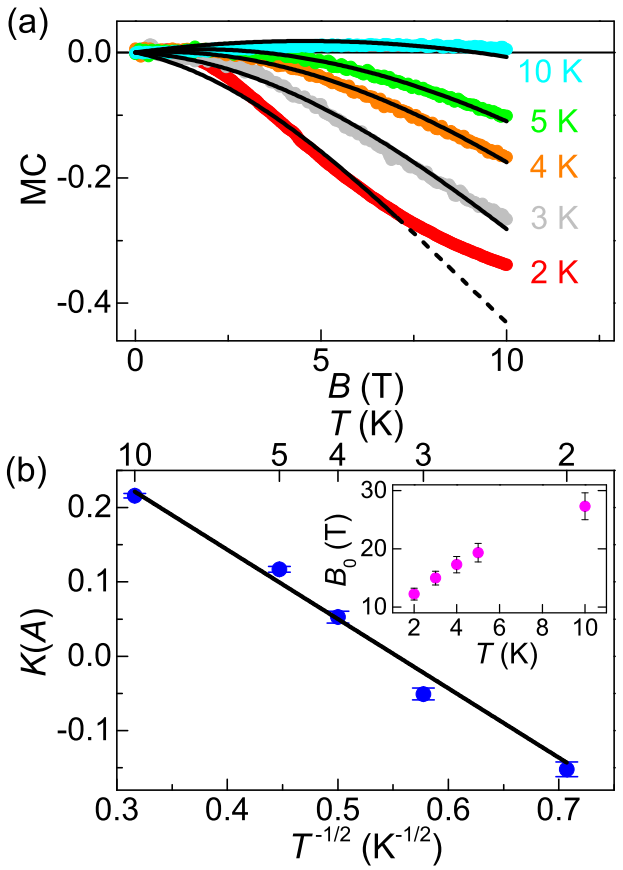

FIG. 4. (a) T-dependent s-SWCNT MC below 10 K exhibits very large negative MC (on the order of 0.10) that monotonically decreases with decreasing temperature. The black fit lines from Eq. 2 show that interference (positive term) and wavefunction shrinkage (negative term) can explain most of the MC behavior of s-SWCNT ensembles. (b) Temperature dependence of the $K(A)$ ratio scales as $T^{-1/2}$. The small value of $K(A)$ (<0.25 for all T) and the $T^{-1/2}$ trend strongly suggest the transport occurs in the weak scattering regime. Inset: B_0 values for all temperatures. When $B>B_0$, the wavefunction shrinkage MC component dominates the interference term.

that occur when an external magnetic field is applied. The first term stems from two negative MC contributions created by wavefunction shrinkage[45] and spin-dependent hopping[47,48], both of which approximately scale as B^2. We expect that the majority of this contribution comes from wavefunction shrinkage, which is expressed as $\ln\left[\frac{\rho(B,T)}{\rho(0,T)}\right]_{\text{orbital}} = \frac{2}{3}\left(\frac{B}{B_0}\right)^2$, where $B_0 = \frac{\sqrt{2}\phi_0}{\pi\xi^2\sqrt{\frac{T_0}{T}}}$, $\phi_0 = \frac{h}{e}$ is the flux quantum, and $\rho(B,T)$ is the B and T-dependent resistivity. The second MC contribution is from the so-called forward interference between two hopping sites[49,50]. In this model, multiple conduction pathways between two points interfere to increase the probability of going from site 1 to site 2, thus generating positive MC. First pioneered by Nguyen et al.[49,50], and then later refined by Schirmacher[51] and Raikh et al.[52], this interference model produces a positive MC that saturates at large B values. In Raikh et al.'s model[52], $\frac{\rho(B,T)}{\rho(0,T)}_{\text{interference}} = 1 - K(A)B/B_0$. Logarithmically adding to the two contributions, $\ln\left[\frac{\rho(B,T)}{\rho(0,T)}\right]_{\text{total}} = \ln\left[\frac{\rho(B,T)}{\rho(0,T)}\right]_{\text{orbital}} + \ln\left[\frac{\rho(B,T)}{\rho(0,T)}\right]_{\text{interference}}$, and remembering that $\text{MC} = \frac{1-\frac{\rho(B,T)}{\rho(0,T)}}{\frac{\rho(B,T)}{\rho(0,T)}}$, we have[52]:

$$\text{MC}_{\text{VRH}} = \exp\left[-\ln\left[1 - K(A)\frac{B}{B_0}\right] - \frac{2}{3}\left(\frac{B}{B_0}\right)^2\right] - 1. \quad (2)$$

Figure 4(a) shows T-dependent MC for the s-SWCNT film along with numerical fits using Eq. 2. The full T-dependent MC data set was simultaneously fit to obtain T-independent values of ξ. For the traces shown in Fig. 4(a), we find $\xi = 2.81 \pm 0.10$ nm best describes the data. In conjunction with our previously determined value of T_0 in 2D $\left[= \frac{13.8}{k_B\xi^2 N(E_F)}\right]$, we obtain $N(E_F) = (2.7 \pm 0.2) \times 10^{15}$ eV^{-1}cm^{-2}.

In addition to finding ξ and $N(E_F)$, fits using Eq. 2 also give insight into the microscopic nature of the scattering process. In Raikh et al.'s analysis of scattering-induced MC in the VRH regime, the T-dependent $K(A)$ parameter varies between 0 (no scattering) to 1.1 (strong scattering). Here, $K(A)$ is a description of scattering strength and is a complicated function A, which is a parameter directly proportional to the electrostatic potential between two hopping sites, V_0[52]: $A = \frac{\pi^{3/2}}{2^{5/2}} N(E_F) V_0 \xi^2 \sqrt{\frac{T_0}{T}}$. As seen in Fig. 4(b), $K(A)$ ranges from ~0.22 at 10 K to ~−0.15 at 2 K, which strongly suggests that carriers undergoing 2D VRH conduction in s-SWCNT ensembles are weakly scattered. In the weak scattering regime, $K(A)$ is approximately equal to $\frac{16}{3\sqrt{\pi}}A$, which is proportional to $\sqrt{\frac{1}{T}}$, as defined above[52]. Thus, the dependence of $K(A)$ on $T^{-1/2}$ shown in Fig. 4(b) adds considerable support for the conclusion that carriers are weakly scattered in this system[52].

In contrast to the negative MC exhibited by the s-SWCNT film, the m-SWCNT ensemble shows a small, positive MC that increases with decreasing T and increasing B. As seen in Fig. 5a, the change in MC with field at high temperatures is linear and small. When T decreases, the positive MC increases until it begins to saturate. At the lowest temperatures (<10 K), the MC saturates at increasingly smaller applied fields, which suggests other effects, such as wavefunction shrinkage or electron-electron interactions[13], become significant. This observation of saturated, positive MC in m-SWCNT films has been previously seen by Yanagi et al.[17] at 2 K. However, unlike our work, T-dependent MC was not investigated, leaving several questions unanswered, such as the nature of the dephasing and the magnitude of the coherence length.

For disordered metallic films[53–56], conduction is weakly

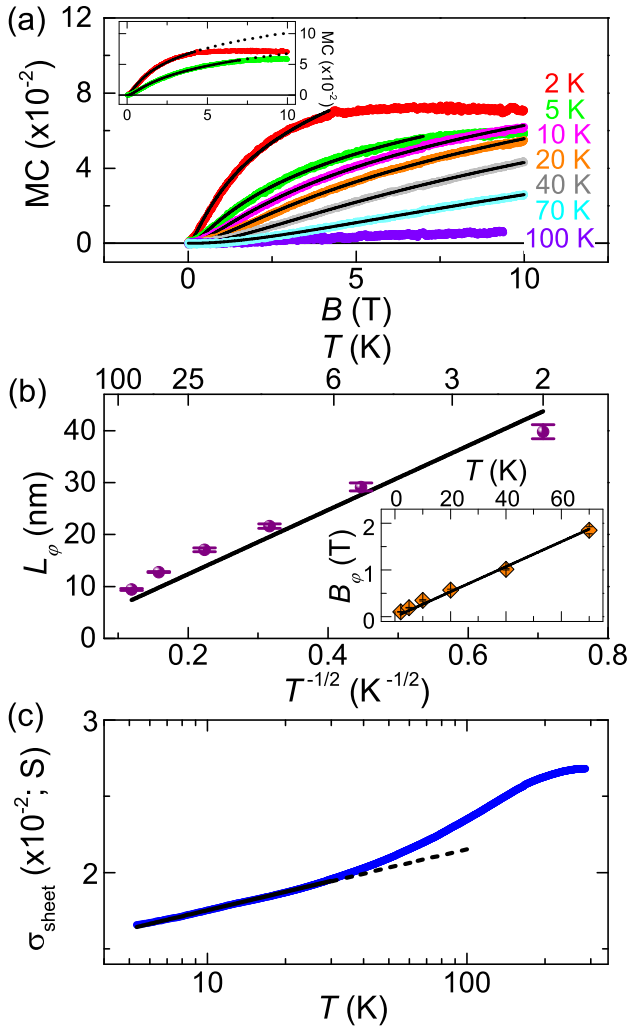

FIG. 5. (a) T-dependent MC for the m-SWCNT film. As T decreases, the MC increases and becomes saturated at increasingly lower B values. The 2DWL mechanism (black lines) fits the MC data well from 2 to 70 K. Inset: MC traces with fits for 2 and 5 K. The dotted black lines show the extrapolated 2DWL MC fit. (b) L_ϕ increases with decreasing T, following a $T^{-1/2}$ behavior from 2 to 70 K. This scaling suggests that the phase decoherence occurs via electron-electron interactions. Inset: The measured values of the coherence field, B_ϕ, show a linear dependence on T. (c) T-dependent sheet conductivity of the m-SWCNT film (blue) follows a 2DWL behavior at low T, as indicated by the black fit line from Eq. 3 (dotted line is the extrapolation out to 100 K).

localized by imperfections in the lattice translational invariance[57,58]. In the WL model, phase-coherent carrier wavefunctions constructively interfere along time-reversed paths augmenting the probability of returning to their original positions[59]. The increased carrier backscattering thus decreases the electrical conduction in disordered metallic films. Scattering via the presence of other carriers, phonons, impurities, and magnetic scatterers destroys this phase coherence, which provides a means for us to measure WL if we know how the scattering time (or length) scales. Typically, it is assumed that the phase decoherence time, τ_ϕ, is equal to $\left[\tau_{\rm in}^{-1} + 2\tau_{\rm s}^{-1}\right]^{-1}$, where $\tau_{\rm in}$ is the inelastic scattering time and is proportional to T^{-p}, $\tau_{\rm s}$ is the magnetic scattering time, and p is a fraction that determines the dominant inelastic scattering mechanism[57–59]. From these relationships, we can obtain a form for $\sigma\,(T)$ in the WL regime, a subject we will return to later.

Although a power-law temperature scaling of $\sigma\,(0,T)$ is predicted in the WL model, T-dependent MC is a more conclusive way to discern and understand WL. Specifically, MC in the WL regime has several distinguishing traits: the MC is positive, it increases with decreasing T, and it has a distinct functional form. These behaviors arise from the broken time-reversal symmetry between interfered partial waves, which suppresses backscattering when a magnetic field is applied perpendicular to the plane of the interference. We note that positive MC has been seen in variety of carbon-based systems, such as pregraphitic carbon[60,61], nanofibers[62], and graphitic and amorphous carbon films[63]. Beyond these studies using carbonaceous materials, 2DWL has been observed in highly doped, aligned nanotube fibers[21], individual multi-wall nanotubes[59], doped SWCNT films[13], and metallic SWCNT bundles[17,64]. Based off of these works and recognizing that the expected B^2 dependence for 3DWL at low fields (and/or high temperatures) does not describe our data[16,65], we focus our attention on 2DWL, which predicts that MC is quantitatively described as[21,58,64]:

$$\mathrm{MC_{2DWL}} = \frac{C}{\sigma\,(0,T)}\frac{e^2}{2\pi^2\hbar}\left[\psi\left(\frac{1}{2}+\frac{B_\phi}{B}\right)+\ln\left(\frac{B}{B_\phi}\right)\right], \tag{3}$$

where C is a constant, ψ is the digamma function, and B_ϕ, the phase coherence field, is equal to $\frac{\hbar}{4eD\tau_\phi} = \frac{\hbar}{4eL_\phi^2}$, where D is the diffusion constant and L_ϕ is the phase coherence length. Although $C = 1$ in the strict theoretical treatment of 2DWL, we take C be a fit parameter here (i.e., $\neq$1) to properly scale the model to our data, since the curvature of the data (determined by B_ϕ) is the main objective of our analysis. Additionally, it should also be noted that we are not dealing with a traditional 2D system, which exhibits translational invariance across the crystal, but a network of 1D wires collected into bundles that define a quasi-2D cylindrical structure. As such, the appropriate model describing our system may not conform to the traditional form of Eq. 3, thus causing C to deviate from 1.

In Fig. 5a, we use Eq. 3 to fit the MC curves from 70 to 2 K taken on the m-SWCNT film. At high T, the fits describe the data well, which suggests that 2DWL is the dominant mechanism in this range. To some extent, this behavior is expected, since even if our metallic film contains narrow-bandgap semiconductors[66], thermal activation of carriers across the meV-sized bandgaps will produce metal-like behavior. However, as T drops (<10 K),

only the low-field range of the MC can be reasonably fit with the 2DWL model, indicating that the metallicity of the film has decreased enough so that wavefunction shrinkage, which is typically seen when carrier localization is present, or electron-electron interactions, which can occur in low-dimensional systems with slow carrier diffusion[13], begin to play a significant roles. The discrepancy with Eq. 3 at low T is highlighted by the dotted lines included on the 2 and 5 K MC traces (inset of Fig. 5a), which show how 2DWL behavior would manifest itself at high magnetic fields without the presence of another transport mechanism. Competition between 2DWL (positive MC) and wavefunction shrinkage (negative MC) may arise from the presence of a freezing out of thermally activated carriers from narrow-bandgap semiconductors.

From the fitting of Eq. 3, we obtain the temperature behavior of B_ϕ (inset of Fig. 5), which we use to determine both L_ϕ and the main dephasing mechanism of the 2DWL transport. B_ϕ is assumed to follow a power-law scaling with T, such that $B_\phi \propto T^p$. Using a single-parameter fit to our values of B_ϕ, we find that p is 0.80, which suggests that electron-electron interactions in either 2D (p=1) or 1D (p=0.67) is the dominant dephasing mechanism. We use $B_\phi(T)$ to calculate the phase coherence length, L_ϕ, of the carriers. As shown in Fig. 5b, L_ϕ increases with reduced temperature rising from $\simeq$10 to $\simeq$40 nm as the temperature decreases from 70 to 2 K. These numbers closely agree with results obtained in doped, pristine SWCNT mats[13], m-SWCNT films[17], and multi-wall carbon nanotubes[21,67]. Importantly, the temperature scaling (fit without any offset parameter) of L_ϕ is shown in Fig. 5b, which follows from $L_\phi \propto \sqrt{\frac{1}{B_\phi}}$ and $p \approx 1$, so $L_\phi \propto T^{-1/2}$.

As noted above, the ambiguity of the dimensionality of the electron-electron dephasing mechanism arises from a value of p that falls between 0.67 and 1. Given the magnitude of L_ϕ is on the order of the bundle diameter, we believe that the phase decoherence from electron-electron interactions is two dimensional. If the electron transport is on the surface of a SWCNT bundle, then this picture make sense. However, it is very reasonable to expect that 1D electron-electron interactions may be dominant. In this paradigm, electron transport occurs along individual nanotubes (or closely grouped nanotubes) in a bundle. Regardless of the exact dimensionality of the dephasing mechanism, the observation of electron-electron interactions has precedent in several other closely related structures, such as iodine-doped polyacetylene[39], pregraphitic nanofibers[62], individual multi-wall carbon nanotubes[59], ensembles of multi-wall carbon nanotubes[67], and doped SWCNTs[13]. This behavior suggests that even at high temperatures, electron-electron interactions play a role in ensemble metallic nanotube electrical transport.

Finally, we return to the T-dependent conductivity of m-SWCNTs shown previously in Fig. 5c. Given we are dealing with a two-dimensional system, we express the $\sigma(0,T)_{\text{sheet}}$ as a sheet conductivity by multiplying conductivity by film thickness. 2DWL theory predicts that $\sigma(0,T)_{\text{sheet}}$ should scale as $\ln(T)$ if no other effects are significant[58]:

$$\sigma(0,T)_{\text{sheet}} = \sigma_0 + \Gamma \frac{pe^2}{2\pi^2\hbar} \ln\left[\left(\frac{T}{T_C}\right)\right], \qquad (4)$$

where σ_0 is from impurity scattering, Γ is a fitting constant, and T_C is the critical temperature. As seen in Fig. 5c, Eq. 4 describes the low temperature behavior of $\sigma(0,T)_{\text{sheet}}$ very well. Deviations from the $\ln(T)$ scaling behavior occur when T goes above $\sim$30 K (indicated by the dashed line) suggesting that a high-T mechanism other than 2DWL may also be affecting carrier transport. We note that the inclusion of a Coulombic interaction correction, often called the Altshuler-Aronov correction[58,68,69], did not improve our description of the data compared to Eq. 4. Though carrier-carrier interactions are likely involved in the zero field, T-dependent transport behavior, their effect in m-SWCNT ensembles manifests itself most prominently the 2DWL dephasing mechanism.

In summary, we systematically studied T- and B-dependent carrier transport using SWCNT ensembles of varying metallicity. We observed distinct magneto-transport behaviors for the metal- and semiconductor-enriched nanotube networks that deepen our understanding of magneto-transport in SWCNT ensembles. Specifically, we ascribe 2D VRH transport to the semiconductor-enriched and pristine SWCNT ensembles. The large, negative MC of the semiconductor SWCNT films at T<10 K reveals contributions from forward interference (positive) and wavefunction shrinkage (negative) from which we estimate that the localization length of the hopping species, ξ, to be 2.81$\pm$0.1 nm and the density of states at the Fermi energy as $(2.7 \pm 0.2) \times 10^{15}$ eV^{-1}cm^{-2}. In contrast to the large, negative MC seen in the s-SWCNT film, a weak, positive MC was observed in the metal-enriched SWCNT sample. We find that this behavior is well-described by a 2DWL mechanism, whose dominant dephasing process occurs via low-dimensional electron-electron interactions over a wide temperature range. From the T-dependent MC, we establish that L_ϕ is tens of nm and scales as $T^{-1/2}$. Importantly, we find that 2DWL is also able to explain $\sigma(0,T)_{\text{sheet}}$ for the m-SWCNTs at low T. Taken together, our results provide deep insights into the magneto-transport mechanisms of SWCNT ensembles, which are increasingly becoming a technologically important carbon material.

ACKNOWLEDGMENTS

The authors thank Matthew Fischer, Chris Leighton, and Angela Hight-Walker for stimulating and productive conversations. XW thanks the National

Natural Science Foundation of China under Grant #11774409. JK acknowledges support from the Department of Energy Basic Energy Sciences through grant #DEFG02-06ER46308, the National Science Foundation through award #ECCS-1708315, and the Robert A. Welch Foundation through grant #C-1509. WDR thanks the Wyoming NASA EPSCoR, NASA Grant #NNX15AK56A and the University of Wyoming School of Energy Resources for financial support for this project.

* wrice2@uwyo.edu; corresponding author.

[1] Z. Yao, C. L. Kane, and C. Dekker, Phys. Rev. Lett. **84**, 2941 (2000).
[2] T. Ando, J. Phys. Soc. Japan **66**, 1066 (1997).
[3] F. Wang, G. Dukovic, L. E. Brus, and T. F. Heinz, Science **308**, 838 (2005).
[4] E. H. Hároz, J. G. Duque, X. Tu, M. Zheng, A. R. H. Walker, R. H. Hauge, S. K. Doorn, and J. Kono, Nanoscale **5**, 1411 (2013).
[5] S. J. Tans, M. H. Devoret, H. Dai, A. Thess, R. E. Smalley, L. J. Geerligs, and C. Dekker, Nature **386**, 474 (1997).
[6] J. Kong, E. Yenilmez, T. W. Tombler, W. Kim, H. Dai, R. B. Laughlin, L. Liu, C. S. Jayanthi, and S. Y. Wu, Phys. Rev. Lett. **87**, 106801 (2001).
[7] J. P. Lu, Phys. Rev. Lett. **79**, 1297 (1997).
[8] A. Y. Kasumov, R. Deblock, M. Kociak, B. Reulet, H. Bouchiat, I. I. Khodos, Y. B. Gorbatov, V. T. Volkov, C. Journet, and M. Burghard, Science **284**, 1508 (1999).
[9] M. Fujii, X. Zhang, H. Xie, H. Ago, K. Takahashi, T. Ikuta, H. Abe, and T. Shimizu, Phys. Rev. Lett. **95**, 065502 (2005).
[10] E. Pop, D. Mann, Q. Wang, K. Goodson, and H. Dai, Nano Lett. **6** (2006).
[11] R. Saito, G. Dresselhaus, and M. Dresselhaus, *Physical Properties of Carbon Nanotubes* (Imperial College Press, 1998).
[12] W. Liang, M. Bockrath, D. Bozovic, J. H. Hafner, M. Tinkham, and H. Park, Nature **411**, 665 (2001).
[13] V. Ksenevich, M. Shuba, and A. Paddubskaya, Medžiagotyra **20**, 126 (2014).
[14] D. Janas, N. Czechowski, Z. Adamus, and T. Gizewski, Appl. Phys. Lett. **112**, 053104 (2018).
[15] G. T. Kim, E. S. Choi, D. C. Kim, D. S. Suh, Y. W. Park, K. Liu, G. Duesberg, and S. Roth, Phys. Rev. B **58**, 16064 (1998).
[16] J. Vavro, J. M. Kikkawa, and J. E. Fischer, Phys. Rev. B **71**, 155410 (2005).
[17] K. Yanagi, H. Udoguchi, S. Sagitani, Y. Oshima, T. Takenobu, H. Kataura, T. Ishida, K. Matsuda, and Y. Maniwa, ACS Nano **4**, 4027 (2010).
[18] J. E. Fischer, H. Dai, A. Thess, R. Lee, N. M. Hanjani, D. L. Dehaas, and R. E. Smalley, Phys. Rev. B **55**, R4921 (1997).
[19] M. Jaiswal, W. Wang, K. A. Shiral Fernando, Y.-P. Sun, and R. Menon, Phys. Rev. B **76**, 113401 (2007).
[20] N. Behabtu, C. C. Young, D. E. Tsentalovich, O. Kleinerman, X. Wang, A. W. K. Ma, E. A. Bengio, R. F. ter Waarbeek, J. J. de Jong, R. E. Hoogerwerf, et al., Science **339**, 182 (2013).
[21] L. Piraux, F. Abreu Araujo, T. N. Bui, M. J. Otto, and J.-P. Issi, Phys. Rev. B **92**, 085428 (2015).
[22] W. D. Rice, R. T. Weber, A. D. Leonard, J. M. Tour, P. Nikolaev, S. Arepalli, V. Berka, A.-L. Tsai, and J. Kono, ACS Nano **6**, 2165 (2012).
[23] W. D. Rice, R. T. Weber, P. Nikolaev, S. Arepalli, V. Berka, A.-L. Tsai, and J. Kono, Phys. Rev. B **88**, 041401(R) (2013).
[24] Q. Zhang, E. H. Hároz, Z. Jin, L. Ren, X. Wang, R. S. Arvidson, A. Lüttge, and J. Kono, Nano Lett. **13**, 5991 (2013).
[25] M. S. Arnold, S. I. Stupp, and M. C. Hersham, Nano Lett. **5**, 713 (2005).
[26] M. S. Arnold, A. A. Green, J. F. Hulvat, S. I. Stupp, and M. C. Hersham, Nature Nanotechnology **1**, 60 (2006).
[27] K. Yanagi, Y. Miyata, and H. Kataura, Appl. Phys. Exp. **1**, 034003 (2008).
[28] E. H. Hároz, W. D. Rice, B. Y. Lu, S. Ghosh, R. H. Hauge, R. B. Weisman, S. K. Doorn, and J. Kono, ACS Nano **4**, 1955 (2010).
[29] J. A. Fagan, M. L. Becker, J. Chun, and E. K. Hobbie, Adv. Mater. **20**, 1609 (2008).
[30] J. Park, P. Deria, J.-H. Olivier, and M. J. Therien, Nano Lett. **14**, 504 (2013).
[31] J. J. Crochet, S. Hoseinkhani, L. Lüer, T. Hertel, S. K. Doorn, and G. Lanzani, Phys. Rev. Lett. **107**, 257402 (2011).
[32] M. J. O'Connell, S. M. Bachilo, C. B. Huffman, V. C. Moore, M. S. Strano, E. H. Hároz, K. L. Rialon, P. J. Boul, W. H. Noon, C. Kittrell, et al., Science **297**, 593 (2002).
[33] F. Wang, D. J. Cho, B. Kessler, J. Deslippe, P. J. Schuck, S. G. Louie, A. Zettl, T. F. Heinz, and Y. R. Shen, Phys. Rev. Lett. **99**, 227401 (2007).
[34] B. Wells, R. Kumar, J. C. L. Reynolds, K. Peters, and P. D. Bradford, Appl. Phys. Lett. **111**, 263102 (2017).
[35] S. H. Jhang and Y. W. Park, Syn. Metals **216**, 72 (2016).
[36] J. F. Woods and C. Y. Chen, Phys. Rev. **135**, A1462 (1964).
[37] L. Halbo and R. J. Sladek, Phys. Rev. **173**, 794 (1968).
[38] L. Essaleh, S. M. Wasim, G. Marín, C. Rincón, S. Amhil, and J. Galibert, J. Appl. Phys. **122**, 015702 (2017).
[39] M. Reghu, K. Väkiparta, Y. Cao, and D. Moses, Phys. Rev. B **49**, 16162 (1994).
[40] H. Gu, J. Guo, X. Yan, H. Wei, X. Zhang, J. Liu, Y. Huang, S. Wei, and Z. Guo, Polymer **55**, 4405 (2014).
[41] R. Rosenbaum, T. Murphy, E. Palm, S. Hannahs, and B. Brandt, Phys. Rev. B **63**, 094426 (2001).
[42] O. Entin-Wohlman, Y. Gefen, and Y. Shapira, J. Phys. C: Solid State Phys. **16**, 1161 (1983).
[43] N. F. Mott, Philosophical Magazine **19**, 835 (1969).
[44] N. Mott, *Conduction in Non-Crystalline Materials* (Oxford University Press, New York, NY USA, 1993), 2nd ed.
[45] B. I. Shklovskii and A. L. Efros, *Electronic Properties of Doped Semiconductors*, Solid-State Sciences (Springer-Verlag, 1984).
[46] A. L. Efros and B. I. Shklovskii, J. Phys. C: Solid State Phys. **8**, L49 (1975).
[47] A. Kurobe and H. Kamimura, J. Phys. Soc. Japan **51**, 1904

(1982).
[48] H. Kamimura and H. Aoki, *The Physics of Interacting Electrons in Disordered Systems* (Clarendon Press, New York, NY USA, 1989), 1st ed.
[49] V. L. Nguyen, B. Z. Spivak, and B. I. Shklovskiĭ, Sov. Phys. JETP **62**, 1021 (1985).
[50] V. L. Nguyen, B. Z. Spivak, and B. I. Shklovskiĭ, JETP Lett. **41**, 42 (1985).
[51] W. Schirmacher, Phys. Rev. B **41**, 2461 (1990).
[52] M. E. Raikh and G. F. Wessels, Phys. Rev. B **47**, 15609 (1993).
[53] G. Bergmann, Phys. Rev. Lett. **49**, 162 (1982).
[54] Z. Ovadyahu and S. Moehlecke, Surf. Sci. **113**, 544 (1982).
[55] D. Abraham and R. Rosenbaum, Phys. Rev. B **27**, 1413 (1983).
[56] G. Bergmann, Phys. Rev. B **28**, 515 (1983).
[57] G. Bergmann, Phys. Rep. **107**, 1 (1984).
[58] P. A. Lee and T. V. Ramakrishnan, Rev. Mod. Phys. **57**, 287 (1985).
[59] L. Langer, V. Bayot, E. Grivei, J.-P. Issi, J. P. Heremans, C. H. Olk, L. Stockman, C. Van Haesendonck, and Y. Bruynseraede, Phys. Rev. Lett. **76**, 479 (1996).
[60] S. Mrozowski and A. Chaberski, Phys. Rev. **104**, 74 (1956).
[61] A. A. Bright, Carbon **17**, 259 (1979).
[62] Y. Wang and J. J. Santiago-Avilés, Appl. Phys. Lett. **89**, 123119 (2006).
[63] A. S. Saleemi, W. Sun, R. Singh, Z. Luo, and X. Zhang, J. Appl. Phys. **121**, 233903 (2017).
[64] J. Z. Cai, L. Lu, W. J. Kong, H. W. Zhu, C. Zhang, B. Q. Wei, D. H. Wu, and F. Liu, Phys. Rev. Lett. **97**, 026402 (2006).
[65] A. Kawabata, Solid State Comm. **34**, 431 (1980).
[66] C. L. Kane and E. J. Mele, Phys. Rev. Lett. **78**, 1932 (1997).
[67] R. Tarkiainen, M. Ahlskog, A. Zyuzin, P. Hakonen, and M. Paalanen, Phys. Rev. B **69**, 033402 (2004).
[68] B. L. Al'tshuler and A. G. Aronov, Sov. Phys. JETP **50**, 968 (1979).
[69] B. L. Al'tshuler, A. G. Aronov, and D. E. Khmelnitsky, J. Phys. C: Solid State Phys. **15**, 7367 (1982).